TECHNICAL MEMORANDUM

197

Sensitivity of forecast error to initial conditions using the adjoint method

F. Rabier, P. Courtier, M. Herveou,
B. Strauss and A. Persson

Research Department

October 1993

European Centre for Medium-Range Weather Forecasts
Europäisches Zentrum für mittelfristige Wettervorhersage
Centre européen pour les prévisions météorologiques à moyen

1. INTRODUCTION

The adjoint equations, as explained by *Le Dimet and Talagrand* (1986), allow to compute efficiently the gradient (or vector of first derivatives) of one output parameter of a numerical weather prediction model with respect to all input parameters. Adjoint equations applications have mainly been to data assimilation and sensitivity problems.

The four-dimensional data assimilation problem can be seen as finding the starting point of a model trajectory which will optimize this trajectory in the sense of being close to the available data. Once an objective criterion J measuring the misfit between the model trajectory and the observations has been defined, the adjoint model gives the gradient of J with respect to the starting point x. This gradient can then be provided to a minimization algorithm which will iteratively find out the best x optimizing the objective function J. The theory and first applications of the method can be found in *Lewis and Derber* (1986), *Talagrand and Courtier* (1987) and *Courtier and Talagrand* (1987). For latest results, see *Zou et al* (1992), or *Thépaut et al* (1993), *Rabier et al* (1993).

The gradient of a diagnostic function J can be interesting as such to give us indications about the sensitivity to input parameters, and indeed adjoint equations have been used for a wide range of sensitivity problems. The sensitivity to model parameters has been investigated for instance by *Hall et al* (1982), *Hall* (1986), *Courtier* (1987) and *Marais and Musson-Genon* (1992). The sensitivity of one aspect of the forecast to initial conditions has been the subject of the study of *Errico and Vukicevic* (1992) on real cases. Their results were confirmed by *Rabier et al* (1992), in which the sensitivity of cyclogenesis to initial conditions was tackled in the context of an idealized flow. They also presented a method to filter the contribution of gravity waves on the gradient of the diagnostic function. It consists in using the adjoint of nonlinear normal mode initialization at the end of the integration of the adjoint model.

Here, we shall investigate the sensitivity of forecast errors to initial conditions. The norm is derived from the quadratic invariant of the primitive equations linearized in the vicinity of a state of rest

$$\|x\|^2 = 1/2 \int_0^1 \iint_\Sigma (\nabla\Delta^{-1}\zeta.\nabla\Delta^{-1}\zeta + \nabla\Delta^{-1}D.\nabla\Delta^{-1}D + R_a T_r (\ln\pi)^2 + (C_p/T_r)T^2) d\Sigma (\partial p/\partial\eta) d\eta$$

where ζ, D, T and π stand for vorticity, divergence, temperature and surface pressure, η is the vertical coordinate, T_r is a reference temperature and R_a, C_p are thermodynamic constants. The diagnostic function is the square norm of the difference between the operational 48 hr forecast and the verifying analysis. In all experiments a T63L31 adiabatic model (with horizontal and vertical diffusion and a surface drag, as in *Buizza*, 1993) has been used. The adjoint integration is performed in the vicinity of an adiabatic trajectory

originated from the ECMWF analysis valid 48 hours before the verification time. As in *Rabier et al* (1992), at the end of the adjoint integration, the adjoint of non linear normal mode initialization is performed. The gradient thus obtained shows which areas and which type of balanced modifications of the initial analysis could have degraded or improved the forecast. The integration of the adjoint model was not performed over periods longer than 48 hours as this has been shown to be a reasonable time limit for the validity of the tangent-linear hypothesis (see *Lacarra and Talagrand*, 1988; *Vukicevic*, 1991 or *Rabier and Courtier*, 1992).

Firstly, from a statistical point of view, the sensitivity of forecast error in the northern hemisphere for the month of January 1993 is investigated. Secondly, on specific cases for which the forecast had been particularly bad on certain areas, the forecast error is tracked by the adjoint method back to its possible origin in the previous analyses.

2. SENSITIVITY OF D+2 FORECAST ERRORS IN THE NORTHERN HEMISPHERE TO INITIAL CONDITIONS OVER THE MONTH OF JANUARY 1993

Fig 1 presents the RMS of the gradients of the diagnostic functions with respect to initial conditions of vorticity at level 11 (around 250 hPa) in panel a), level 18 (around 500 hPa) in panel b) and at level 26 (around 850 hPa) in panel c). The inner product with respect to which this gradient is presented is the inner product defined by

$$<x,y>=\Sigma_i\Sigma_l\omega_i x_i^l y_i^l$$

where the summation extends over all the horizontal levels l and all the grid-points i with ω_i representing the Gaussian weight at grid-point i, i.e. the percentage of the globe surface occupied by this grid-point. To compute the change in the diagnostic function J caused by a change in the initial condition x, one should calculate

$$\delta J=<\nabla J,\delta x>=\Sigma_i\Sigma_l\omega_i\nabla J_i^l\delta x_i^l$$

At all levels, one can notice stronger gradients over the oceans than over the continents which is consistent with better initial conditions due to better data coverage over the continents.

Another basic statistical tool has been used to interpret further these results. The occurrences of large gradients are plotted in Figs 2 and 3: number of days out of the 31 days for which the gradient has been above (Fig 2) or below (Fig 3) a given threshold which is taken as a value corresponding to approximately half of observed gradients maxima and minima (+5 and -5 10**10). In Fig 2 (panels a), b) and c)) correspond to levels 11, 18 and 26 as previously), one can see the areas for which more than 4 times out of 31, the forecast error at day 2 would have been significantly smaller if the analysis had been slightly more cyclonic (less anticyclonic). Similarly in Fig 3, one can see the areas for which more than 4 times out of 31, the forecast at day 2 would have been significantly improved.

Looking at Figs 1, 2 and 3, one can see that the high RMS observed over the Atlantic Ocean are mainly due to analyses being not cyclonic enough (in general, larger number of occurrences in Fig 3 for large negative gradients than in Fig 2 for large positive gradients). However, this is not strictly true as, at low levels (Figs 2 and 3, panels c at 850 hPa), the situation is more balanced over the eastern Atlantic for which 10 analyses have been not cyclonic enough and 10 analyses have been too cyclonic.

Similarly, the high RMS observed over the Pacific Ocean are mainly due to analyses being too cyclonic, with again a more balanced situation at low levels for the western Pacific.

Over sensitive cases, it can then be said that generally, an analysis more anticyclonic over the eastern Pacific and more cyclonic over the western Atlantic would improve the two-day forecast.

One can also notice that the relatively high values of RMS over Africa at 250 hPa (around 20°N, 20°E) and over the western Pacific (around 50°N, 150°W) on Fig 1, panel a) correspond to a few analyses which had been too cyclonic (Fig 2, panel a)).

As for the high RMS value over North-Canada at 75°N, 100°W , it does not correspond to a large occurrence on either Fig 2 or Fig 3. Actually, it corresponds only to two days of very high sensitivity.

Fig 4 shows the average over the month of January of the 250 hPa (panel a)) and 500 hPa (panel b)) geopotential height. Comparing with Fig 1, panels a) and b) which represent the RMS of gradients at 250 hPa and 500 hPa, one can note a good correspondence between the sensitive areas and the oceanic jets, both where the geopotential isolines are very tight (maxima of the jets) and in the diffluence areas located in the eastern parts of these jets. In a barotropic model, *Bouttier* (1993) has showed that a large growth in error variance was indeed found in the same type of areas.

One can also try to link these sensitive areas to regions where the analysis error is supposed to be large. In data assimilation, we usually have more information on the first-guess (6-hour forecast) error variance as it is directly used as input to the analysis. We will then compare Fig 1 to first-guess error statistics, which are not supposed to be very different from analysis error statistics. In Fig 5 are presented two independent estimations of first-guess error variance at 500 hPa. Panel a) shows a typical variance chart for a winter day as estimated by the optimal interpolation system. Panel b) shows what is obtained by computing the standard-deviation of differences between 24 and 48 hour forecasts verifying at the same time, over a period of 3 months (December 1989 to February 1990). The result can be thought of as representing forecast error variance and the method, used at NMC for evaluating first-guess statistics, is described in *Rabier and McNally* (1993). Above 30°N, the agreement between Fig 1, panel b) and Fig 5, panels a) and b) is good,

with relative minima over the continents and maxima over the oceans. The best agreement can be found between statistics computed by forecast differences (Fig 5b) and sensitive areas (Fig 1b). Below 30°N, although the OI estimate shows large errors in the tropics, this feature is not present in either the forecast error estimated by forecast differences or in the gradients RMS. It could be that indeed the analysis and first-guess errors are large in this area, but the model does not diverge away from it, so that two trajectories started 24 or 48 hours previously are quite similar and also analyses and two-day forecasts are quite similar.

When looking at the vertical variation of the RMS of gradient on Fig 6, one notices significant variation. Furthermore, the day to day variability is significant (+-25%), with, in addition, a few exceptional cases. The average over the 31 cases is presented in Fig 7. Fig 8 presents the vertical variation of the contribution of vorticity to the diagnostic function (rotational part of the kinetic energy of the error multiplied by the layer depth) for the individual cases of January 1993, and Fig 9 presents the average. The maximum is at the jet level whereas the maximum of sensitivity is located in the mid and low troposphere. This is consistent with the results of *Rabier et al* (1992) and also with the structures of optimal unstable modes (*Buizza*, 1993). However, one should normalize these results by the relative uncertainty in the initial conditions. Even if one m/s error on the wind field leads to a greater change in the diagnostic function when applied at 800 hPa rather than at 200 hPa, there is more chance to have larger errors at the jet level than at lower levels. Statistics computed using the NMC method (*Rabier and McNally*, 1993) show that the vorticity error standard-deviation is around 1.8-1.9 s^{-1} between levels 20 to 31, although it reaches 2.5-2.6 s^{-1} at the levels 10-15.

Fig 10 presents the temporal variation with respect to days of the diagnostic function which is the forecast errors square norm (dark solid line), of the square norm of the gradient summed over all levels and all variables (dashed line) and of the RMS of the gradient with respect to vorticity at level 26 (light solid line). All curves are normalised and of average 1. It is clear that there is little day to day variability in the forecast error norms. However, the sensitivity to initial conditions can vary a lot (by as much as a factor 4). There is no apparent correlation with the day to day variability of the medium range scores (Fig 11).

2. TRACKING BACK THE FORECAST ERROR TO ANALYSIS PROBLEMS ON TWO CASES

In this part of the study, we will still use the energy to measure the diagnostic function, but this energy will be computed over a limited area only, this area varying according to the particular meteorological situation. As a consequence the order of magnitude of the diagnostic functions J can vary quite a lot, and to properly normalize the gradients it seemed appropriate to present those with respect to the inner product

$$\langle x,y\rangle = \Sigma_i \Sigma_l J \Delta p_l \omega_i x_i^l y_i^l$$

in which the order of magnitude of J is included. Furthermore, at each level l, we multiply by the layer

depth in hPa (as in the computation of the diagnostic function itself), so that it corresponds to a real three-dimensional spatial integration. It should be noted that this factor varies from about 25 hPa at the jet level to about 35 hPa in the mid-troposphere, down to just below 10 hPa for the lowest level.

The relative change in the diagnostic function will then be given by

$$\delta J/J = <\nabla J/J, \delta x> = \Sigma_i \Sigma_l \delta p_l \omega_i \nabla J_i^l \delta x_i^l$$

For the study of forecast errors at ranges exceeding 48 hours, it was decided to split the adjoint integration in several 48 hour steps, starting from newly computed diagnostic functions at every step. This is because the validity of the tangent-linear hypothesis on which the adjoint calculation is based, is known to break down after about two days (*Lacarra and Talagrand*, 1988; *Vukicevic*, 1991; *Rabier and Courtier*, 1992). For example, the sensitivity of a D+4 forecast error at day 4 to the analysis at day 0 will be studied first as the sensitivity of a D+2 forecast error at day 4 to the D+2 forecast at day 2 from which it originates. This first step will indicate which area was sensitive to the D+2 forecast started from the analysis at day 0. We will then proceed, after selection of an appropriate area, and after computation over this area of the D+2 forecast error to the sensitivity of this D+2 forecast error from day 0 to the analysis at day 0.

In all cases, the maximum of sensitivity is located in the mid-low troposphere, around 700 to 900 hPa. The gradient charts will then mainly be presented at the representative level 26 (850 hPa) which is among the most sensitive (unless otherwise stated).

2.1 Bad forecast for the period 9-10 April 1993 over North Sea and Scandinavia

Around 9-10 April 1993, a blocking pattern developed over the North Sea and Scandinavia, which was not captured correctly until day 2-3. The forecast from 5 April 1993 gave a very bad forecast at days 4-5, but the problem was already present in the forecasts from 3 April 1993 at days 6-7.

We first considered the problem as starting from 5 April. In Fig 12, the forecast error at day 4 (forecast from the 5th minus analysis for the 9th) is presented in terms of vorticity at level 26 (850 hPa). The forecast is seen to be too cyclonic over the North Sea. The area chosen to compute the diagnostic function (forecast from the 5th minus analysis for the 9th) is represented in Fig 13: it is the area named NS for North Sea (5°W-15°E, 65°N-50°N).

The adjoint model was integrated backwards from the 9th to the 7th, following the trajectory starting from the 2-day forecast from the 5th valid for the 7th. The gradient produced is presented in terms of vorticity in Fig 14, panel a). The corresponding forecast error (2-day forecast from the 5th minus analysis for the

7th) is shown in Fig 14, panel b). One can see that the forecast too cyclonic slightly west of Ireland, associated with an area of strong positive gradient, could indeed cause an error two days later.

Now, another area was chosen for the situation the 7th: it is the area illustrated in Fig 13 by IRL for Ireland (35°W-5°W, 65°N-45°N). The diagnostic function (forecast from the 5th minus analysis for the 7th) was computed and the adjoint model was integrated backwards from the 7th to the 5th, following the trajectory starting from the analysis for the 5th. The gradient produced is presented in terms of vorticity at levels 18 (500 hPa) and 31 (1009 hPa) in Fig 15, panels a) and b). One can compare panel a) with panels c) and d) which represent the perturbations added to the initial conditions of the Monte-Carlo ensemble forecasts starting from the 5th giving the best scores over the North-Sea area for the 9th. These are perturbations to be added to the 500 hPa geopotential field. The common pattern between the two perturbation fields displayed in panels c) and d) is a succession of positive and negative anomalies over the Atlantic. On the one hand, a positive increment in the ensemble means the geopotential field should have been higher to give better forecasts. On the other hand, a positive gradient means that a negative vorticity increment would have improved the forecast. It would then be consistent to find approximately the same pattern in both types of charts, sensitivity and perturbation charts. Comparing panels c) and d) with panel a), one can note a relatively good correspondence between the patterns: positive south of Nova Scotia, negative east of Newfoundland, positive south of Iceland and negative in the area (30°W,30°N). This indicates that, indeed, adding a perturbation following the sensitivity pattern 5 April would improve the score of the nonlinear forecast 4 days later over the North Sea. In Fig 15 panel e), the corresponding analysed MSL pressure with available observations can be compared with the sensitivity chart displayed in panel b) for the lowest model level. Nothing looks really wrong in the analysis compared with the available data. However, the analysis could be wrong in data-void areas. In the area 50°-55°N, 30°W, one can see that if the ridge had been more pronounced (negative increment in vorticity), the forecast would have been improved thanks to the positive gradient. Indeed, this area is lacking some observations and a stronger ridge could have been manually drawn based on the existing data. In the area 30°-40°N, 30°W, one can see that if the pressure low had been extended (positive increment in vorticity), the forecast would have been improved due to the negative gradient. This area is missing sufficient data to be sure of the exact pattern there. A too strong vorticity pattern over Northern mid-Atlantic and a too weak vorticity pattern over Southern mid-Atlantic may then be suspected to be the cause of the bad forecast.

The problem can also be investigated as starting from the 3rd. The 6-day forecast error pattern from the 3rd (not shown) is very similar over the North sea to the 4-day forecast error pattern from the 5th. The area NS in Fig 13 is then chosen to compute the diagnostic function (forecast from the 3 minus analysis for the 9th).

The adjoint model was integrated backwards from the 9th to the 7th, following the trajectory starting from the 4-day forecast from the 3rd valid for the 7th. The gradient produced is presented in terms of vorticity in Fig 16, panel a). The corresponding forecast error (4-day forecast from the 3 minus analysis for the 7th) is shown in Fig 16, panel b). As before, one can see that the forecast too cyclonic slightly west of Ireland, associated with an area of strong positive gradient, could indeed cause an error two days later.

The area IRL was again chosen for the 7th situation. The diagnostic function (forecast from the 3 minus analysis for the 7th) was computed and the adjoint model was integrated backwards from the 7th to the 5th, following the trajectory starting from the 2-day forecast from the 3rd valid for the 5th. The gradient produced is presented in terms of vorticity in Fig 17, panel a). The corresponding forecast error (2-day forecast from the 3 minus analysis for the 5) is shown in Fig 17, panel b). Comparing the two panels of Fig 17, one can note some correspondence between an area of strong positive gradient south of Iceland and a positive error.

The area ISL (shown in Fig 13) was then chosen to compute the last diagnostic function (40°W-15°W, 65°N-45°N). The diagnostic function (forecast from the 3rd minus analysis for the 5th) was computed and the adjoint model was integrated backwards from the 5th to the 3rd, following the trajectory starting from the analysis for the 3rd. The gradient produced is presented in terms of vorticity in Fig 18, panel a). In Fig 18, panel b) the initialised analysis increments are presented, in panel c) the corresponding analysed MSL pressure with available observations and in panel d) the analysed MSL pressure 12 hours later for the 4th at 0Z with available observations.

The first noticeable aspect of the gradient presented in Fig 18 panel a) is its intensity. The sensitivity appears to be much stronger with respect to the analysis for 3/4/93 than what was obtained for 5/4/93 in Fig 15, which strongly suggests that the problem really started on that date. Comparing Fig 18, panels a) and b), one notes that two increments at (40°N, 60°W) and (45°N, 45°W) are acting in the right direction, as their signs are opposite to those of the corresponding gradient. Indeed, having larger increments of this type would have helped decrease the forecast error. In panel c), these increments are seen to be associated with respectively a deepening of a low south of Nova Scotia and a more marked ridge east of Newfoundland. According to the available data, these features could have been even more pronounced. 12 hours later, new observations (Fig 18, panel d)) again confirm that the low should be deeper than it really is in the successive analyses, although we lack information about the ridge further east. Again, one can compare the gradient pattern with the output of the Monte-Carlo simulation. Just one member of the ensemble of the 3rd was scoring more than 50% at day 6 over the North Sea. Its perturbation pattern for the geopotential at 850 Hpa is presented in Fig 18 panel e). The negative perturbation located South of Nova-Scotia corresponds to the one of the sensitivity main features.

The low south of Nova Scotia corresponds to a jet located along the coast of the USA. In an OD memorandum (20/4/93) Anders Persson suspected the problem of the bad forecasts to originate from a bad description of this jet the 3rd at 12Z. Here, we concentrated more on the lower levels as this is where the maximum of the sensitivity takes place, but one of the two factors (vorticity maximum south of Nova Scotia) we found to correspond to Anders' conclusions at upper levels.

2.2 Bad forecast from 12 September 1992

As explained in a OD memorandum (19/09/92) from Anders Persson, the forecast originated from the 12/9/92 which hit Europe at day 3 was particularly bad, with anomaly correlation scores of MSL pressure scoring only 0.38. The error pattern was already present at day 2, and we studied the sensitivity of this error to the analysis.

The forecast error at day 2 is presented in Fig 19. The negative error west of Ireland has been captured in the diagnostic function choosing the area EAT for East Atlantic illustrated in Fig 13 (35°W-5°W, 60°N-45°N). The adjoint model was integrated backwards from the 14th to the 12th, following the trajectory starting from the analysis for the 12th. The gradient produced is presented in terms of vorticity in Fig 20, panel a). In Fig 20, panel b) the corresponding vorticity analysis is presented. One can clearly relate the negative gradient south-east of Nova Scotia with the positive vorticity pattern present in the analysis, although the locations are not perfectly identical. Again, this fits the conclusions from Anders attributing the bad forecast to an underestimated and possibly slightly mislocated low south of Nova Scotia.

3. CONCLUDING REMARKS

The adjoint method seems to be useful as a sensitivity tool. Firstly, we have shown that the technique was giving perfectly reasonable results in a statistical sense, when studying the sensitivity of 48hr forecast error over the northern hemisphere with respect to initial conditions over the month of January 1993. The sensitivity is seen to be particularly intense in the lower levels, and over the oceanic mid-latitudes. Generally, the analysis is found to be too anticyclonic over the Atlantic Ocean and too cyclonic over the Pacific Ocean. Secondly, the approach applied to individual cases helped to focus our attention directly on the sensitive areas. On the two cases studied, our conclusions and those from OD converged.

Of course, the method is limited. From a theoretical point of view, the limitation comes from the validity of the tangent-linear hypothesis which is thought to be around two days. From a practical point of view, the model used in this study is a degraded model compared to the operational one, with a lower truncation and only simplified physics. Using a full truncated trajectory and a simplified adjoint model could improve the accuracy of the method. But, even as such, the tool revealed its efficiency in these simple examples.

4. ACKNOWLEDGEMENTS

MetOps section staff kindly helped with charts displaying observations. Thomas Petroliagis provided useful information and material about Monte-Carlo products.

5. REFERENCES

Buizza, R, 1993: Impact of a simple vertical diffusion scheme and of the optimization time interval on optimal unstable structures. ECMWF Tech Memo No 192, February 1993.

Courtier, P, 1987: Application du contrôle optimal à la prévision numérique en météorologie. Thèse de doctorat de l'université de Paris VI.

Courtier, P and O Talagrand, 1987: Variational assimilation of meteorological observations with the adjoint vorticity equation- Part II. Numerical results. Q J Roy Meteorol Soc, 113, 1329-1347.

Errico, R M and T Vukicevic, 1992: Sensitivity analysis using an adjoint of the PSU/NCAR mesoscale model. Mon Wea Rev, 120, 1644-1660.

Hall, M C G, 1986: Application of adjoint sensitivity theory to an atmospheric general circulation model. J Atmos Sci, 43, 2644-2651.

Hall, M C G, D G Cacuci and M R Schlesinger, 1982: Sensitivity analysis of a radiative-convective model by the adjoint method. J Atmos Sci, 39, 2038-2050.

Lacarra, J-F and O Talagrand, 1988: Short range evolution of small perturbations in a barotropic model. Tellus, 40A, 81-95.

Le Dimet, F-X and O Talagrand, 1986: Variational algorithms for analysis and assimilation of meteorological observations. Tellus, 38A, 97-110.

Lewis, J M and J C Derber, 1985: The use of adjoint equations to solve a variational adjustment problem with advective constraints. Tellus, 37A, 309-322.

Marais, C and L Musson-Genon, 1992: Forecasting the surface weather elements with a local dynamical-adaptation method using a variational technique. Mon Wea Rev, 120, 1035-1049.

Persson, A, 1992: Possible causes of the low quality forecasts from 12-14 September 1992. Operations Department Memorandum O/MOP/22, 19 September 1992.

Persson, A, 1993: A probable cause of the bad ECMWF forecasts 5-6 April 1993. Operations Department Memorandum O/MOP/22, 20 April 1993.

Rabier, F and P Courtier, 1992: Four-dimensional assimilation in the presence of baroclinic instability. Q J Roy Meteorol Soc, 118, 649-672.

Rabier, F, P Courtier and O Talagrand, 1992: An application of adjoint models to sensitivity analysis. Beitr Phys Atmosph, 65, 177-192.

Rabier, F, P Courtier, J Pailleux, O Talagrand and D Vasiljevic, 1993: A comparison between four-dimensional variational assimilation and simplified sequential assimilation relying on three-dimensional variational analysis. Q J Roy Meteorol Soc, 119, 845-880.

Rabier, F and T McNally, 1993: Evaluation of forecast error covariance matrix. ECMWF Tech Memo No 195, September 1993.

Talagrand, O and P Courtier, 1987: Variational assimilation of meteorological observations with the adjoint vorticity equation- Part I Theory. Q J Roy Meteorol Soc, 113, 1311-1328.

Thépaut, J-N, D Vasiljevic, P Courtier and J Pailleux, 1993: Variational assimilation of conventional observations with a multilevel primitive equation model. Q J Roy Meteorol Soc, 119, 153-186.

Vukicevic, T, 1991: Nonlinear and linear evolution of initial forecast errors. Mon Wea Rev, 119, 1603-1611.

Zou, X, I M Navon and F-X Le Dimet, 1992: Incomplete observations and control of gravity waves in variational data assimilation. Tellus, 44A, 273-296.

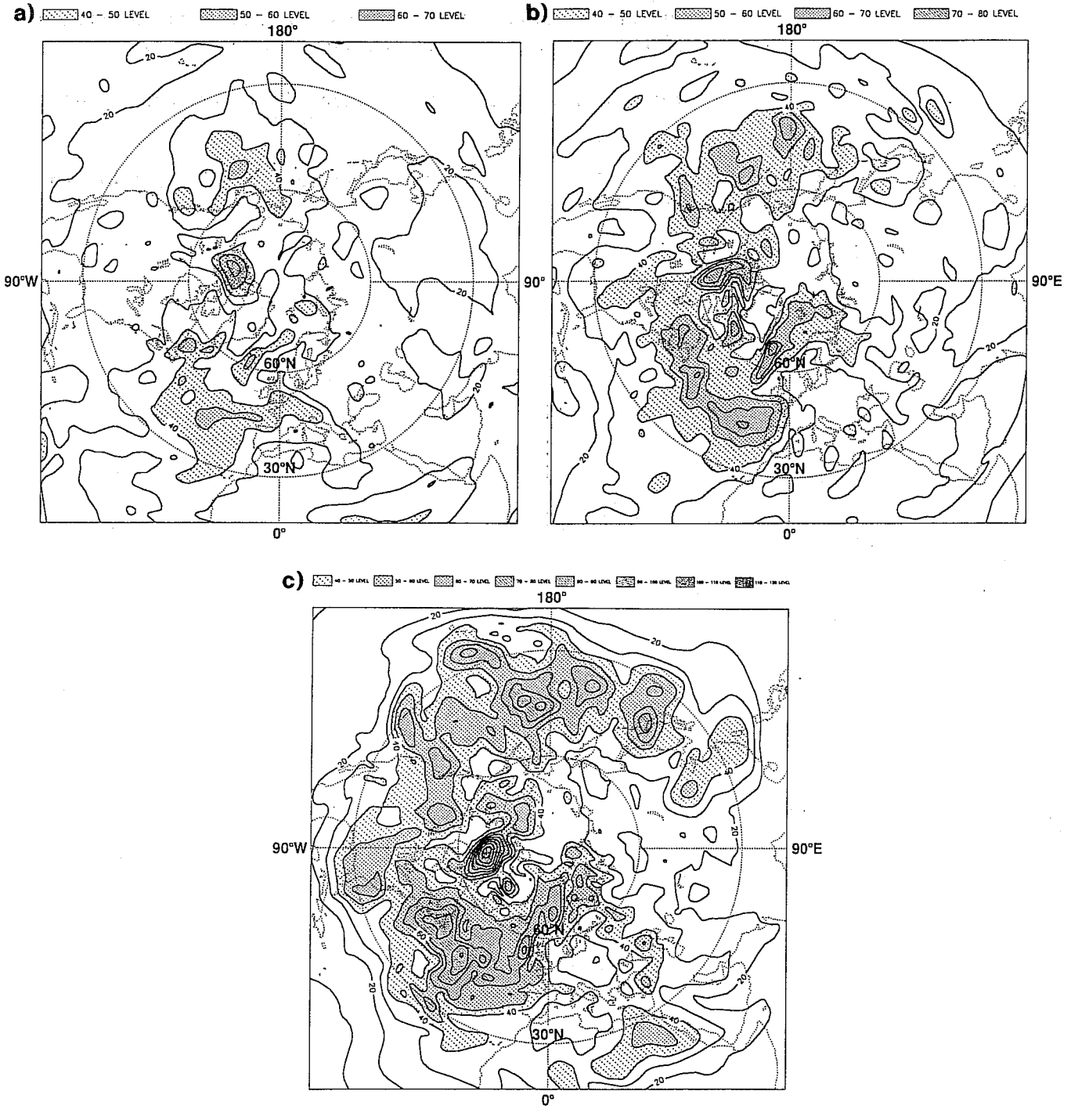

Fig 1 RMS of gradients of 48 hr-forecast error with respect to vorticity in the analysis, computed over January 1993, at level 11 (250 hPa) in panel a), level 18 (500 hPa) in panel b) and level 26 (850 hPa) in panel c).

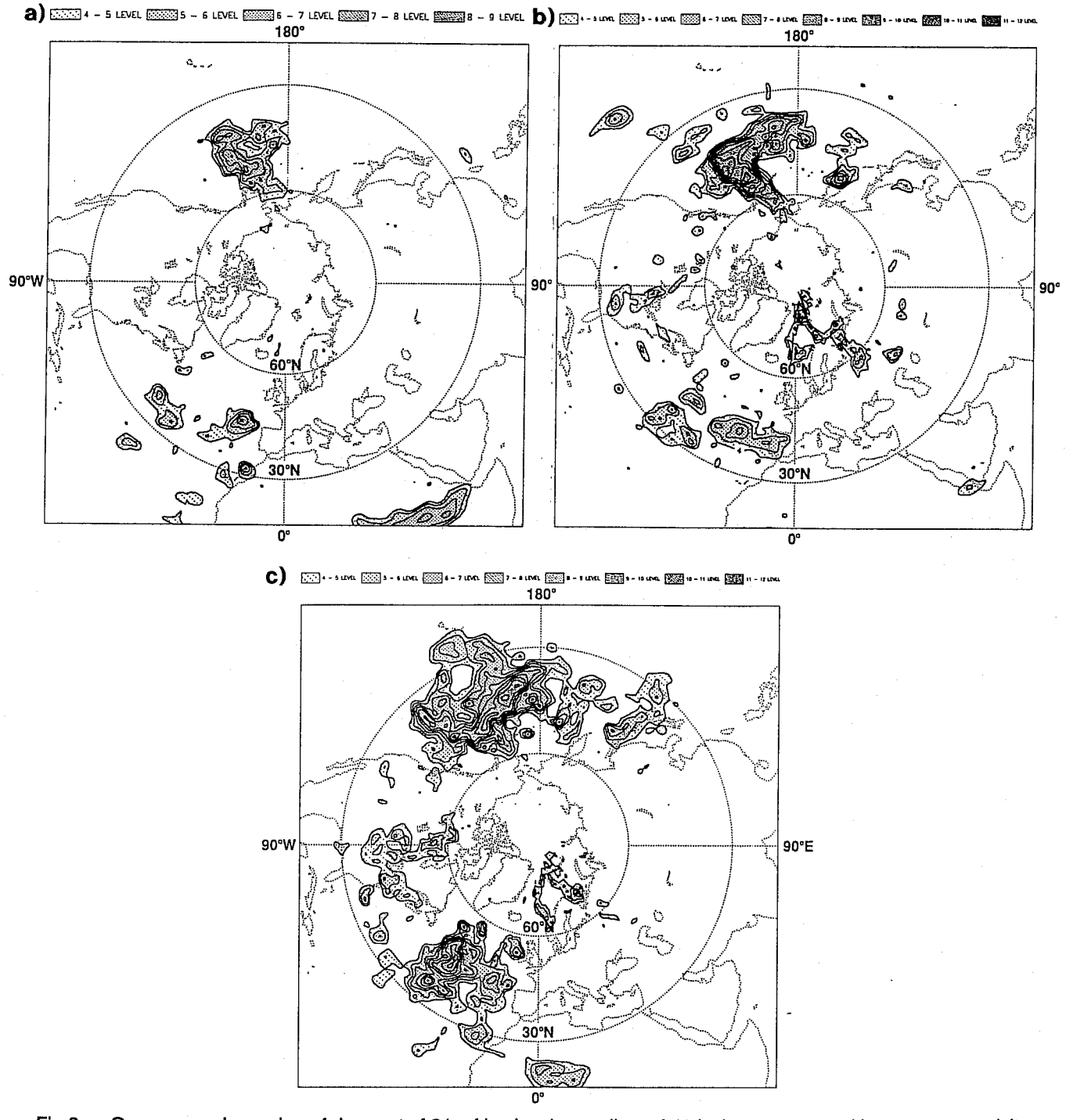

Fig 2 Occurrences in number of days out of 31, of having the gradient of 48 hr-forecast error with respect to vorticity bigger than a threshold of 5 10**10, at levels 11 (panel a), 18 (panel b) and 26 (panel c).

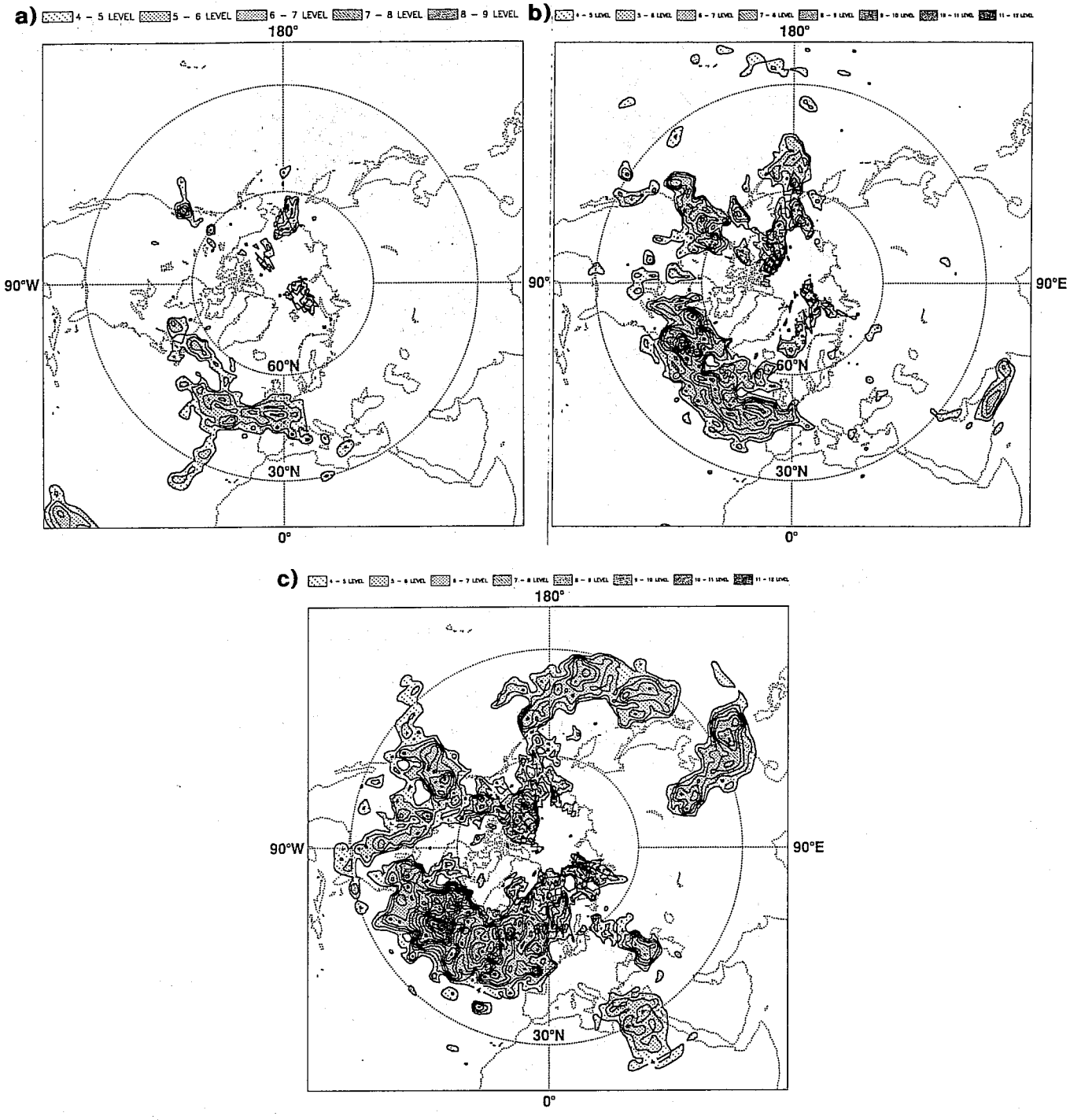

Fig 3 Occurrences in number of days out of 31, of having the gradient of 48 hr-forecast error with respect to vorticity smaller than a threshold of -5 10**10, at levels 11 (panel a), 18 (panel b) and 26 (panel c).

a) ECMWF Analysis VT: Friday 1 January 1993 12z
250 hPa geopotential

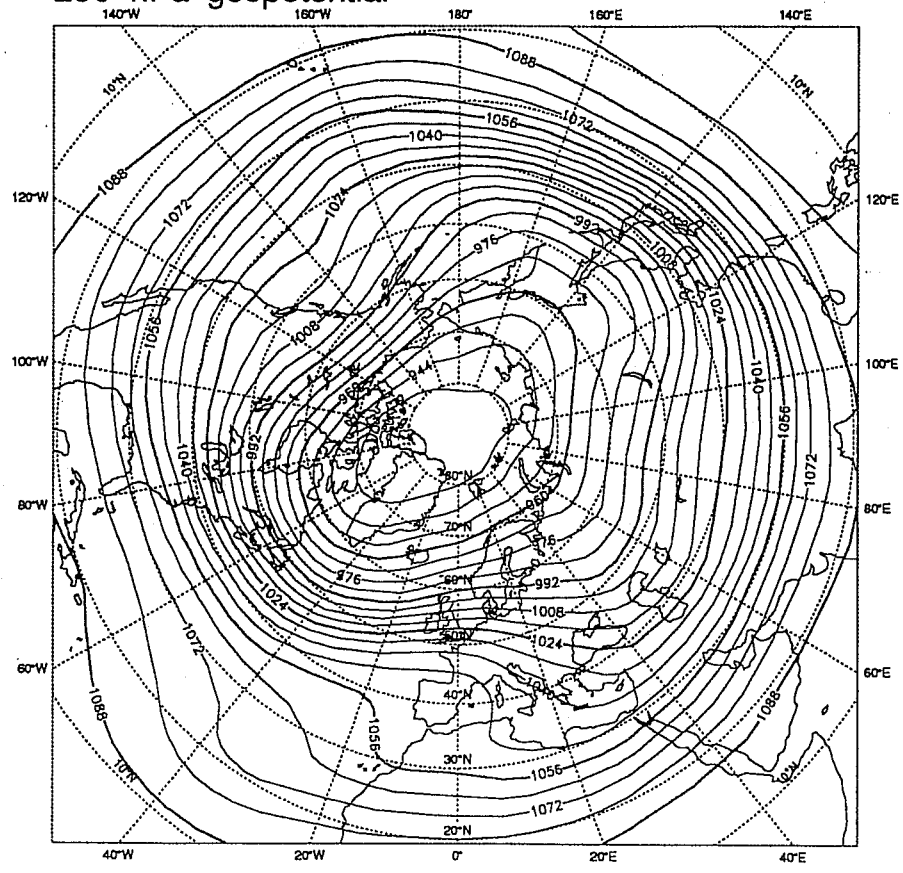

b) ECMWF Analysis VT: Friday 1 January 1993 12z
500 hPa geopotential

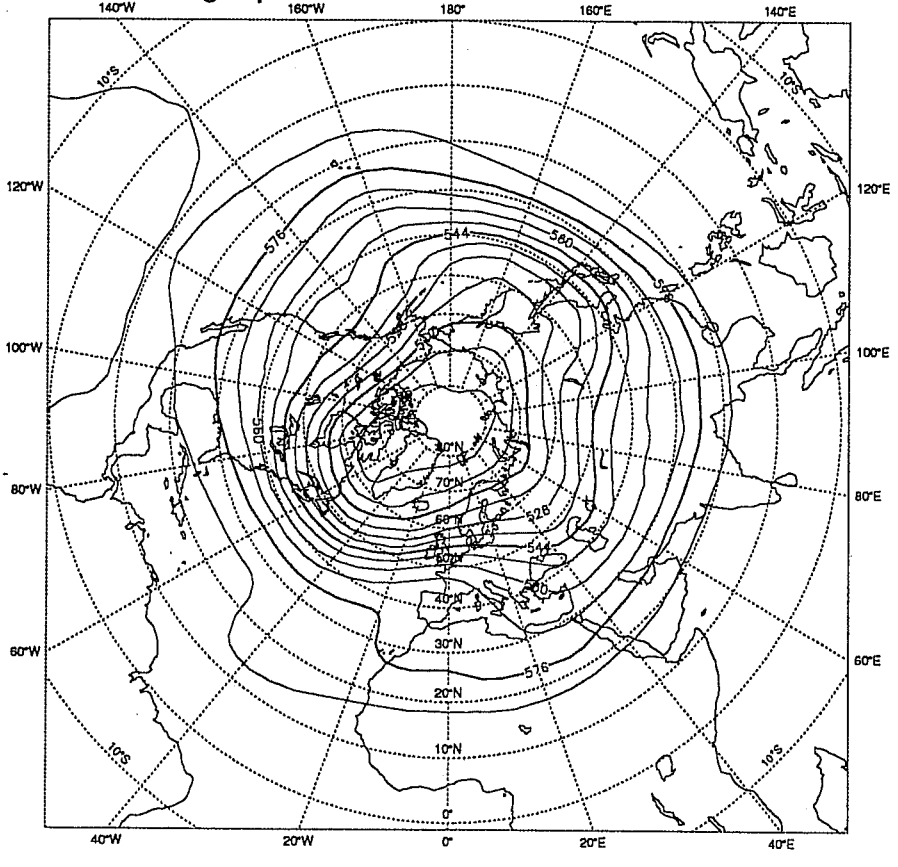

Fig 4 Geopotential height fields averaged over January 1993 at levels 250 hPa (panel a) and 500 hPa (panel b).

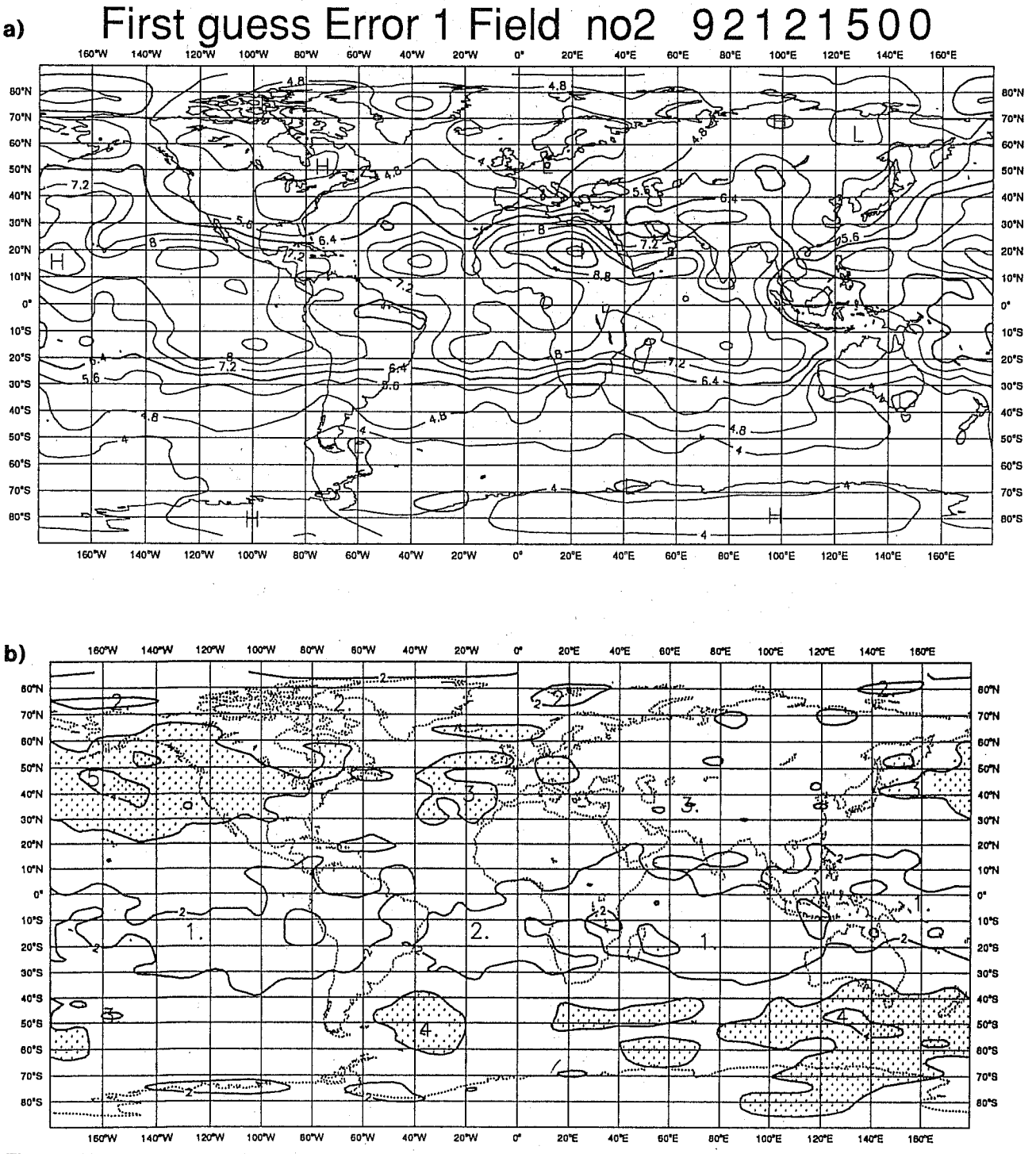

Fig 5 Forecast error estimates. Panel a): example of first-guess error standard-deviation as used in Optimal Imterpolation, for a winter day, for the wind field at 500 hPa (u or v component). Panel b): forecast error standard-deviation as computed by the NMC method for winter 89-90, for the u component of the wind at level 11 (500 hPa).

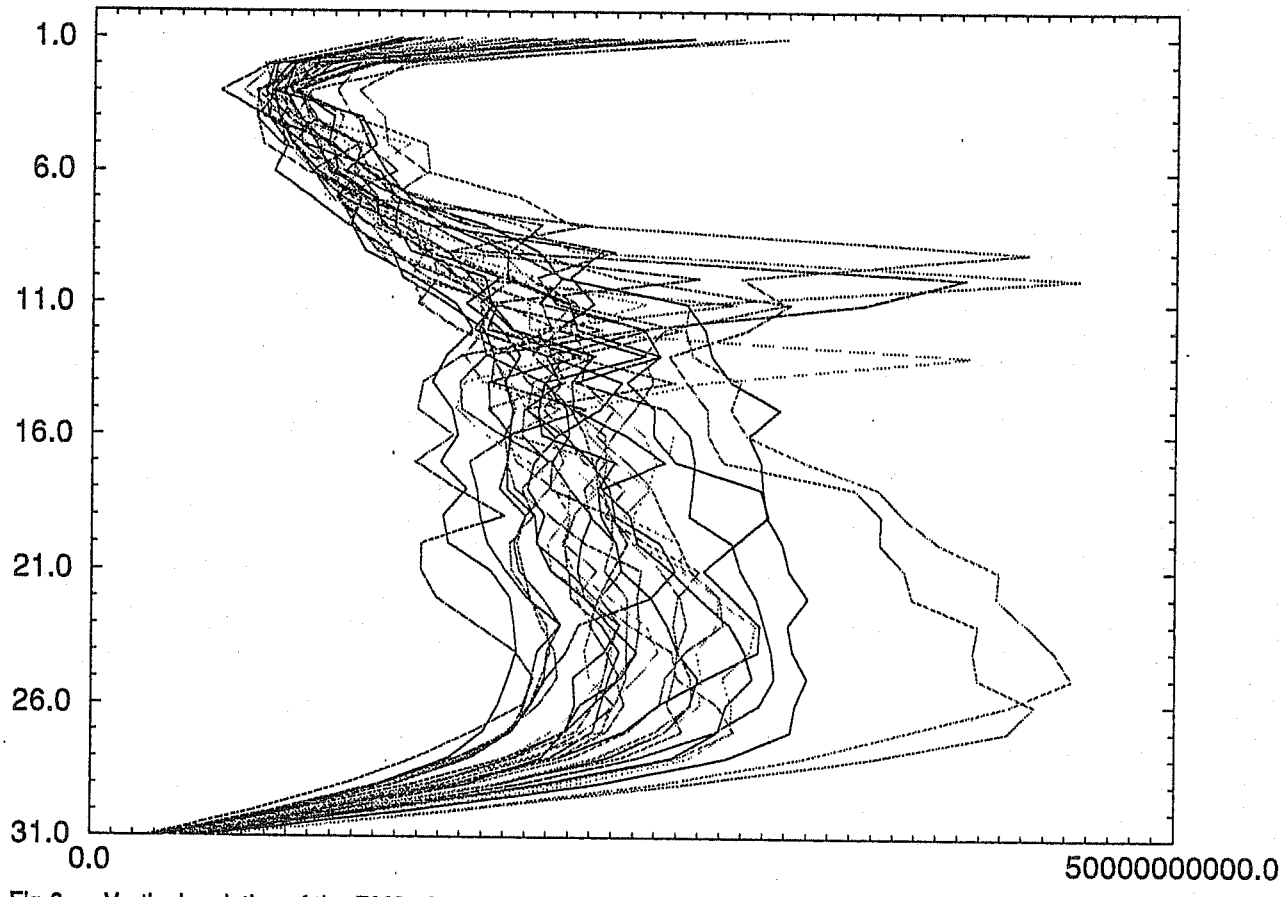

Fig 6 Vertical variation of the RMS of gradient of the 48-hr forecast error with respect to vorticity. All individual cases for the month of January 1993. Vertical scale: model level.

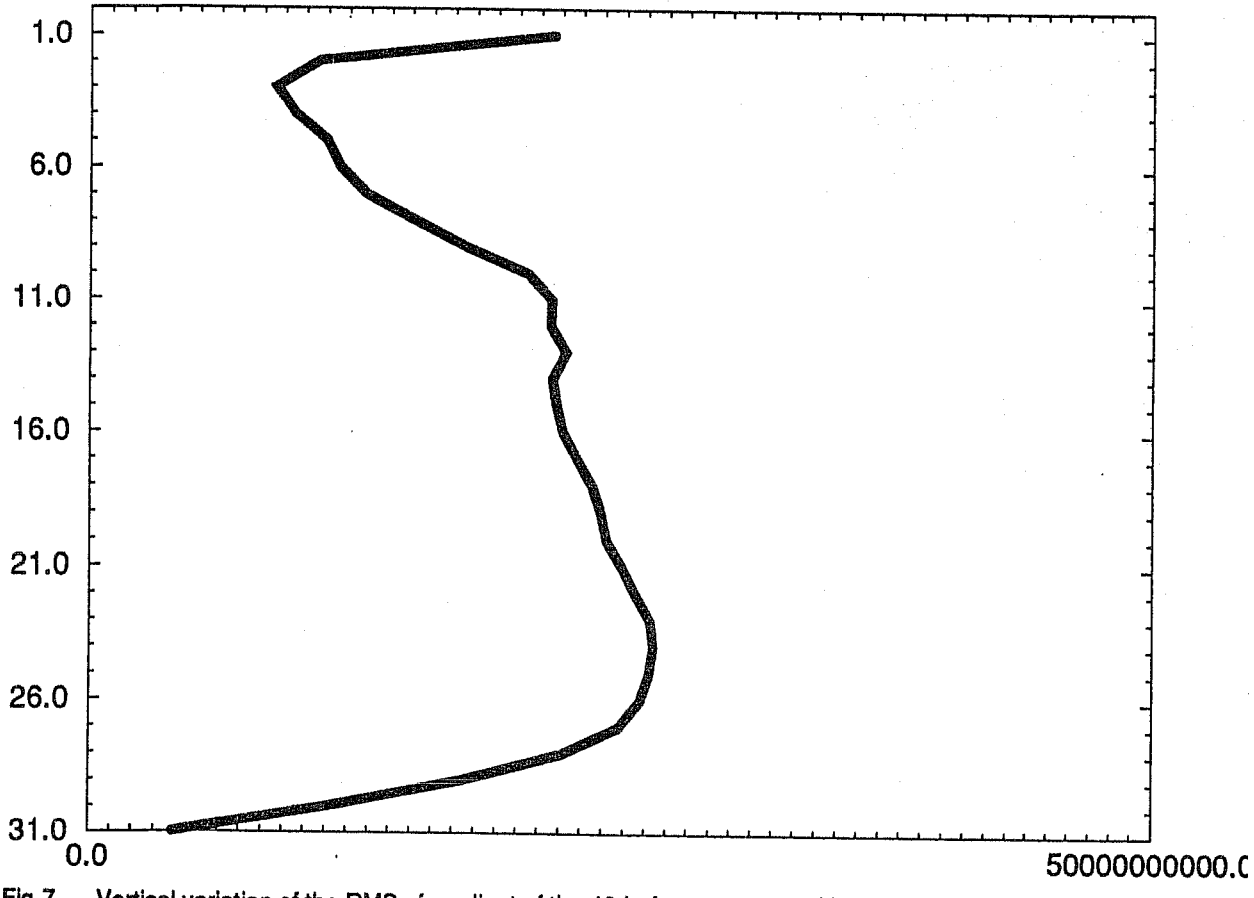

Fig 7 Vertical variation of the RMS of gradient of the 48-hr forecast error with respect to vorticity, for the average over the month of January 1993. Vertical scale: model level.

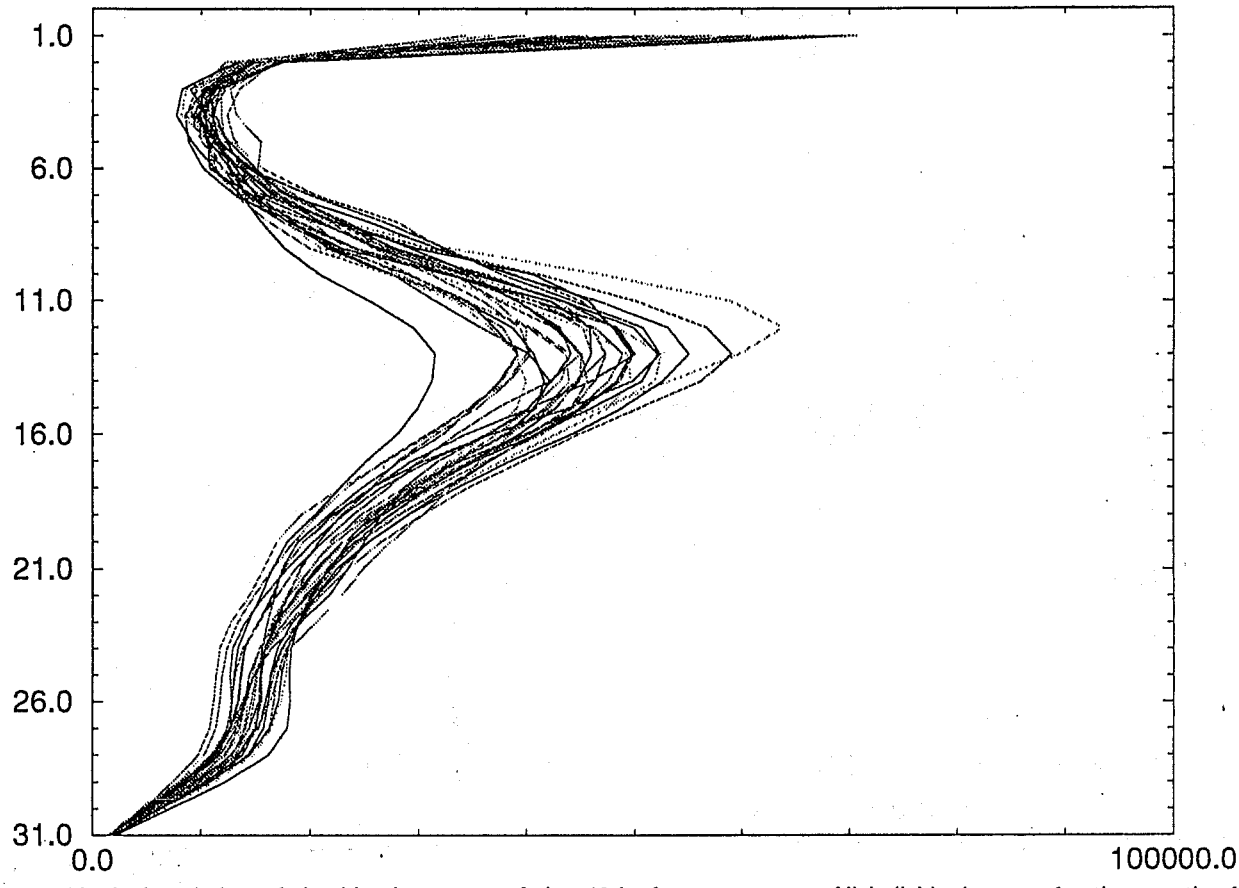

Fig 8 Vertical variation of the kinetic energy of the 48-hr forecast error. All individual cases for the month of January 1993. Vertical scale: model level.

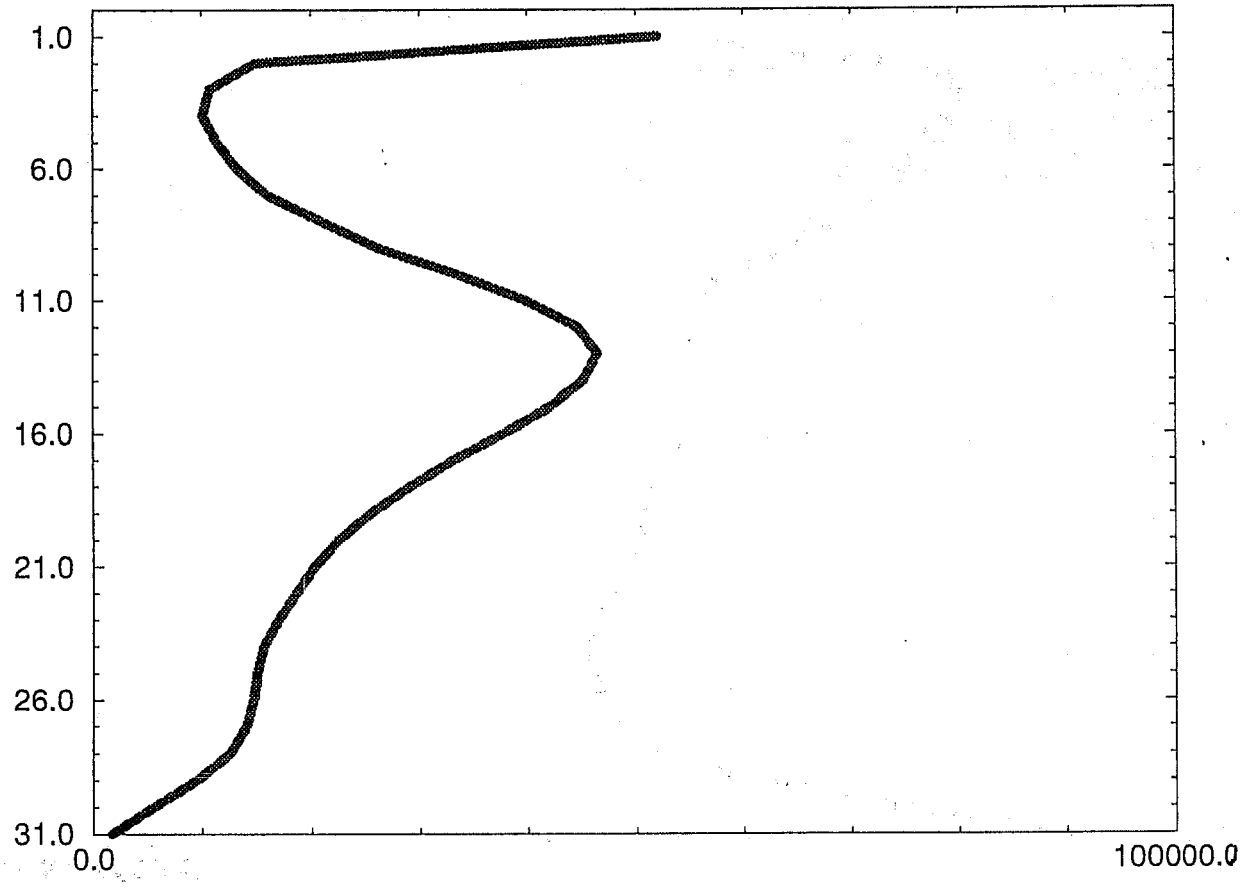

Fig 9 Vertical variation of the kinetic energy of the 48-hr forecast error, for the average over the month of January 1993. Vertical scale: model level.

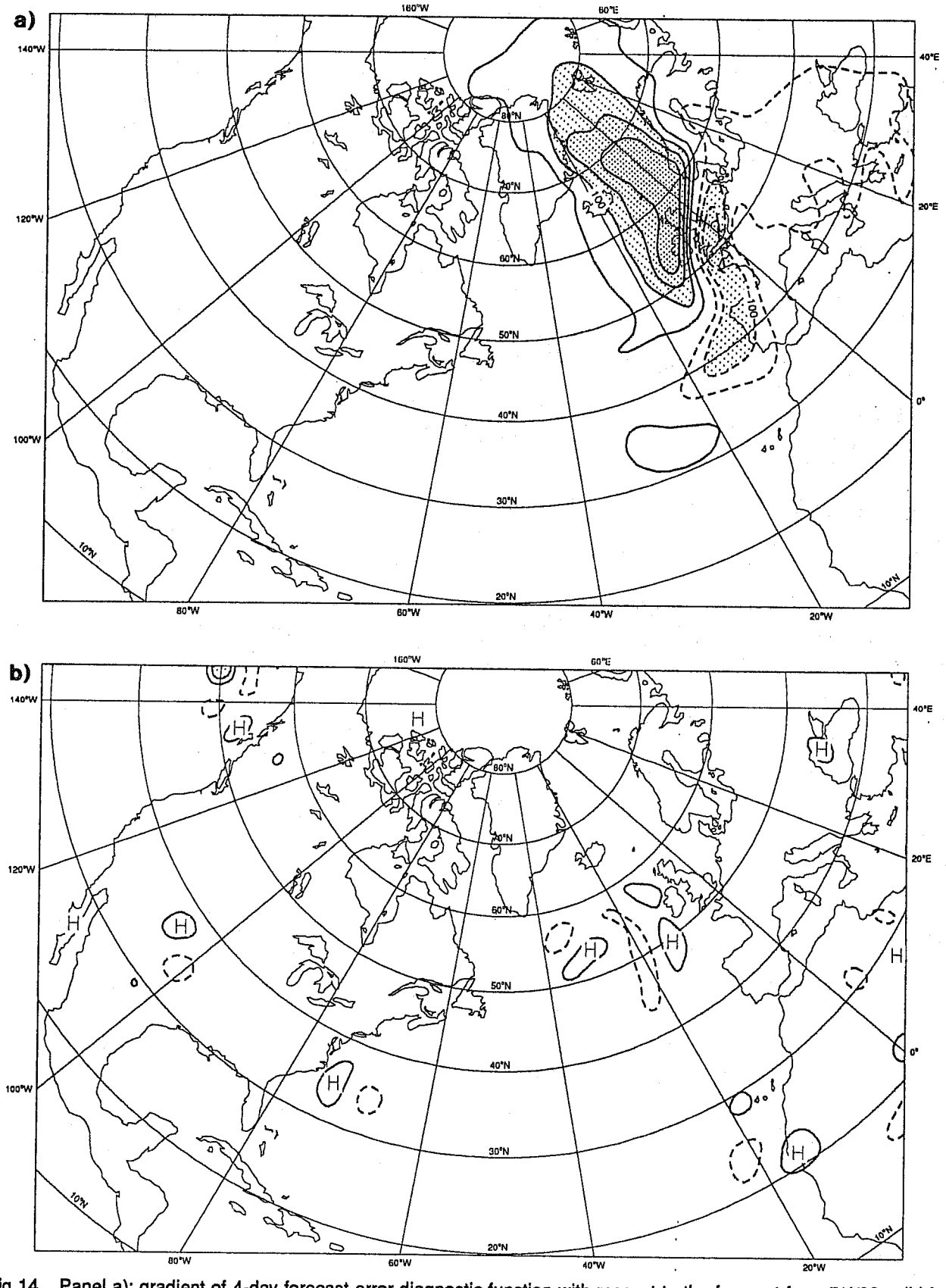

Fig 14 Panel a): gradient of 4-day forecast error diagnostic function with respect to the forecast from 5/4/93 valid for 7/4/93 (vorticity at level 26). Panel b): 2-day forecast error for 7/4/93, 12Z, for vorticity at level 26 (850 hPa).

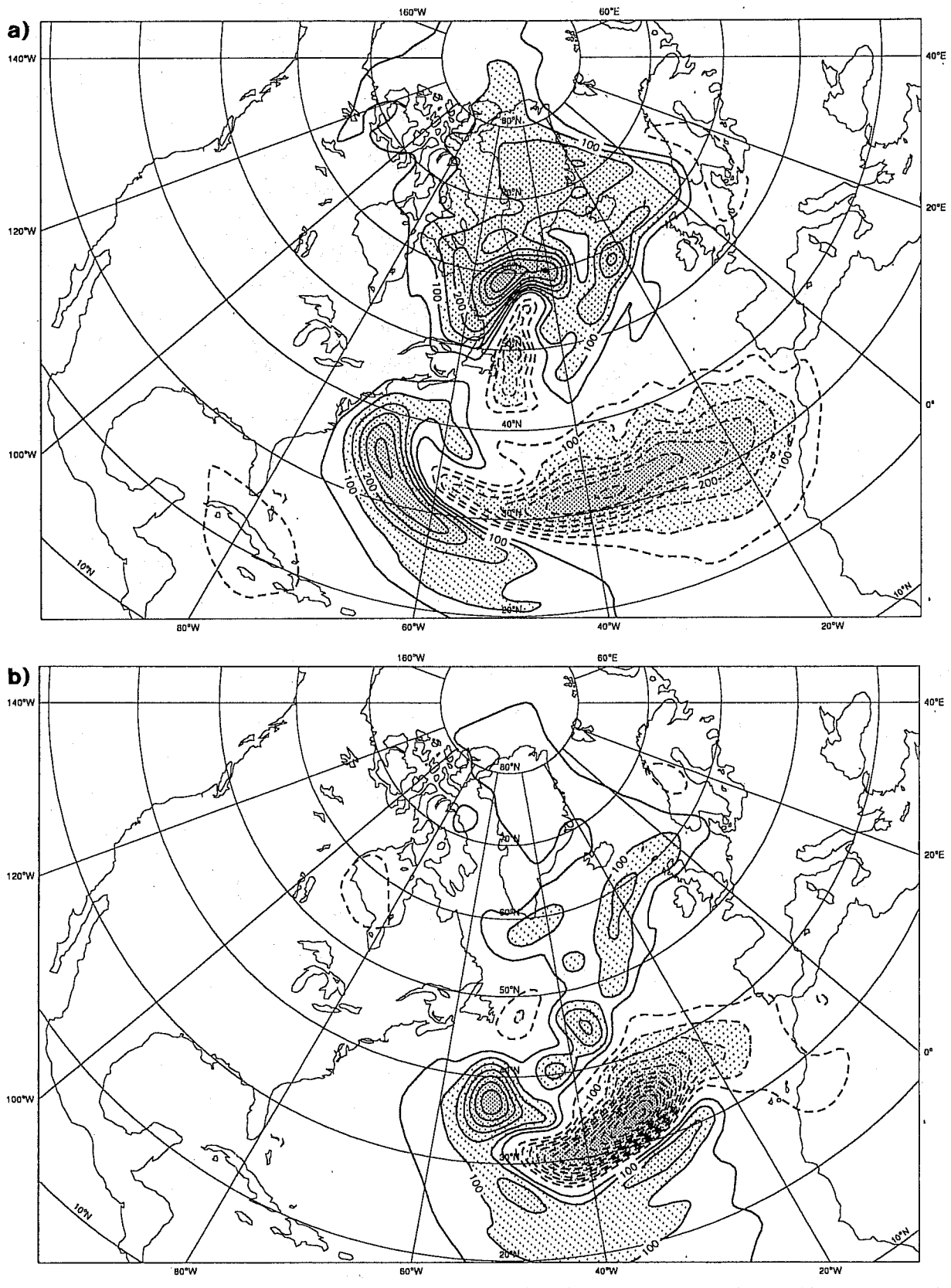

Fig 15 Panel a): gradient of 2-day forecast error diagnostic function with respect to the analysis valid for 5/4/93 (vorticity at level 18). Panel b): gradient of 2-day forecast error diagnostic function with respect to the analysis valid for 5/4/93 (vorticity at level 31). Panels c) and d): initial perturbations added to the control of the Monte-Carlo system at 5/4/93 for the geopotential at 500 hPa which lead to the two best scores over the North-Sea for the 9/4/93. Panel e): Analysed MSL pressure for 5/4/93, with corresponding observations.

c)

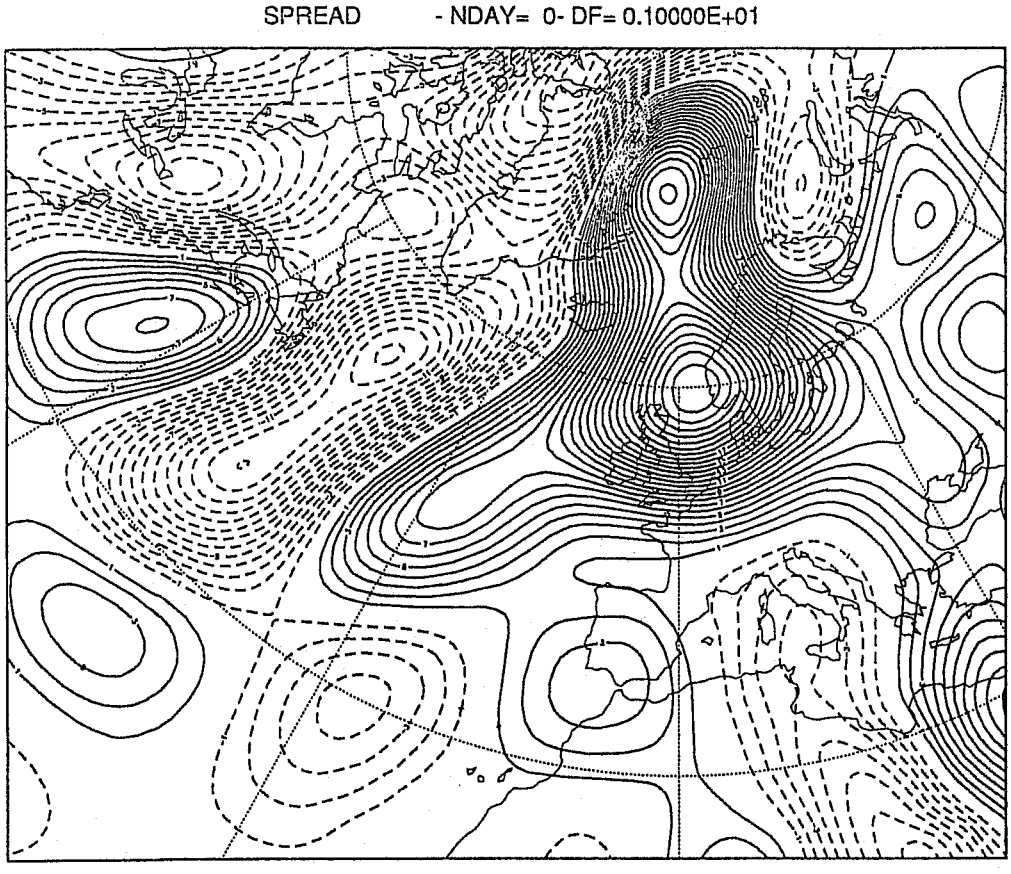

d)

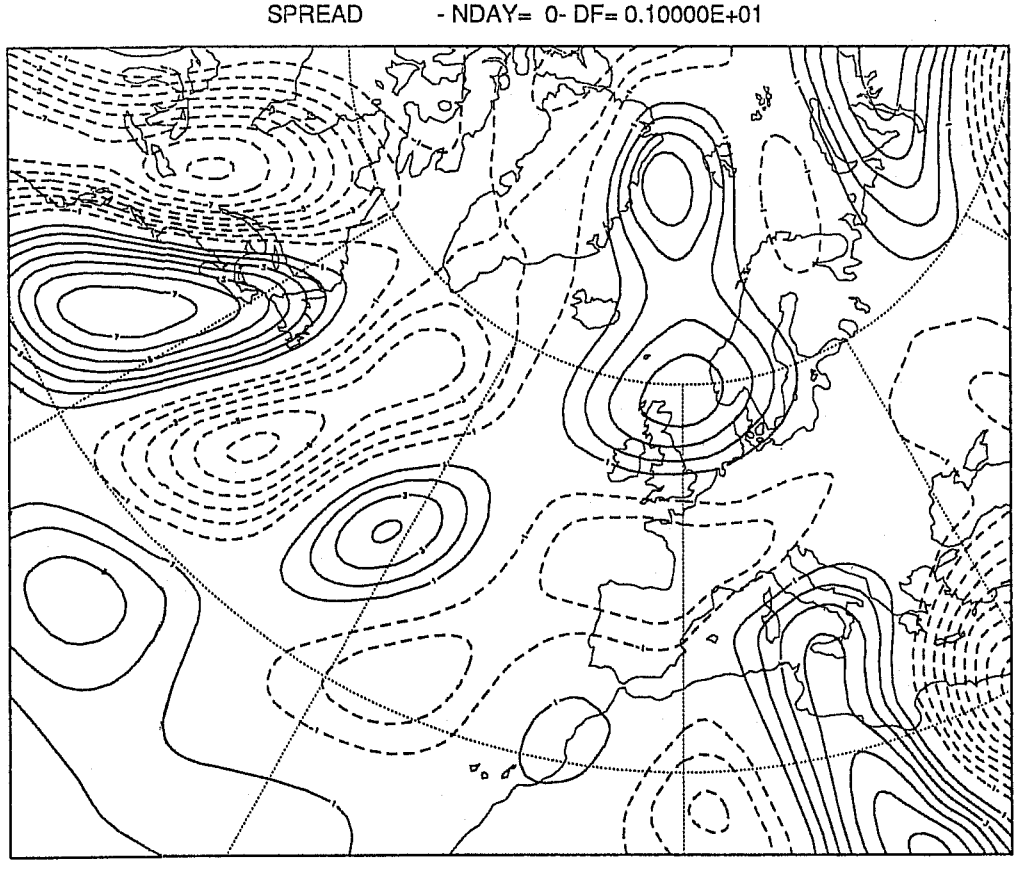

Fig. 15 continued

c)

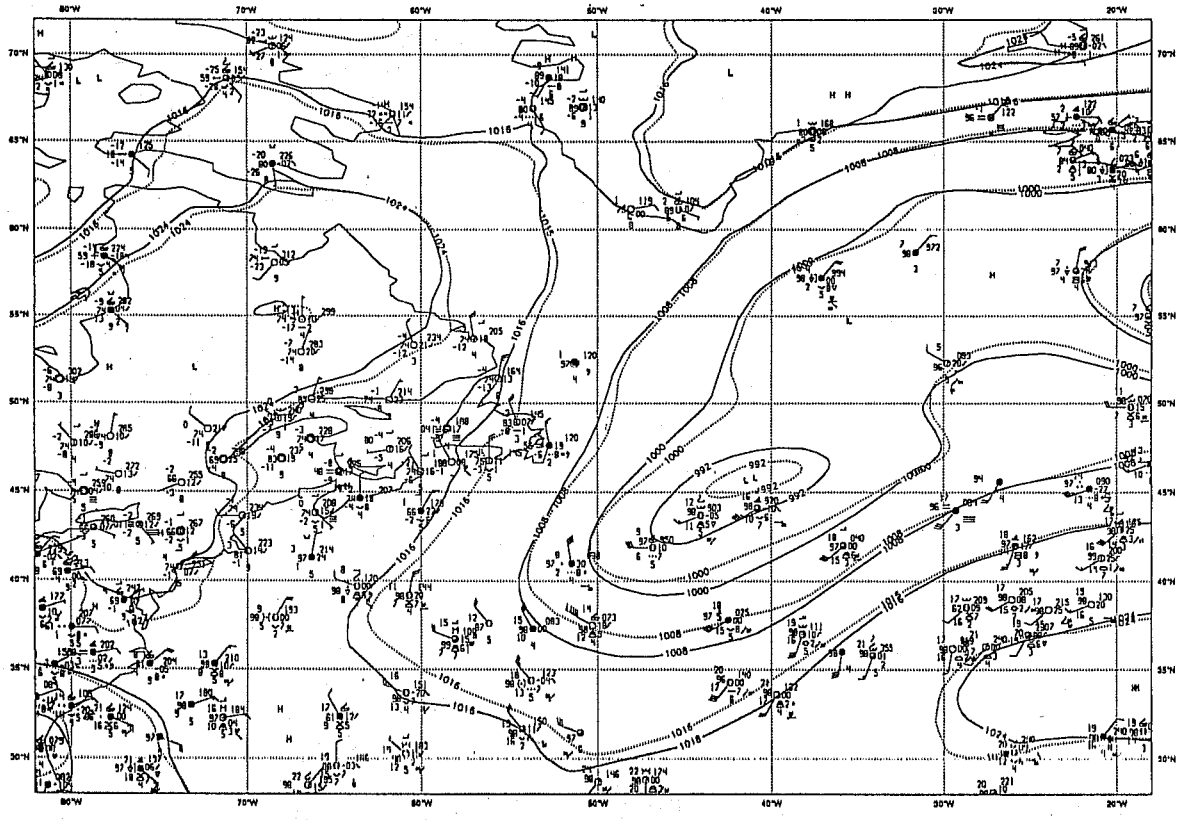

Fig. 15 continued

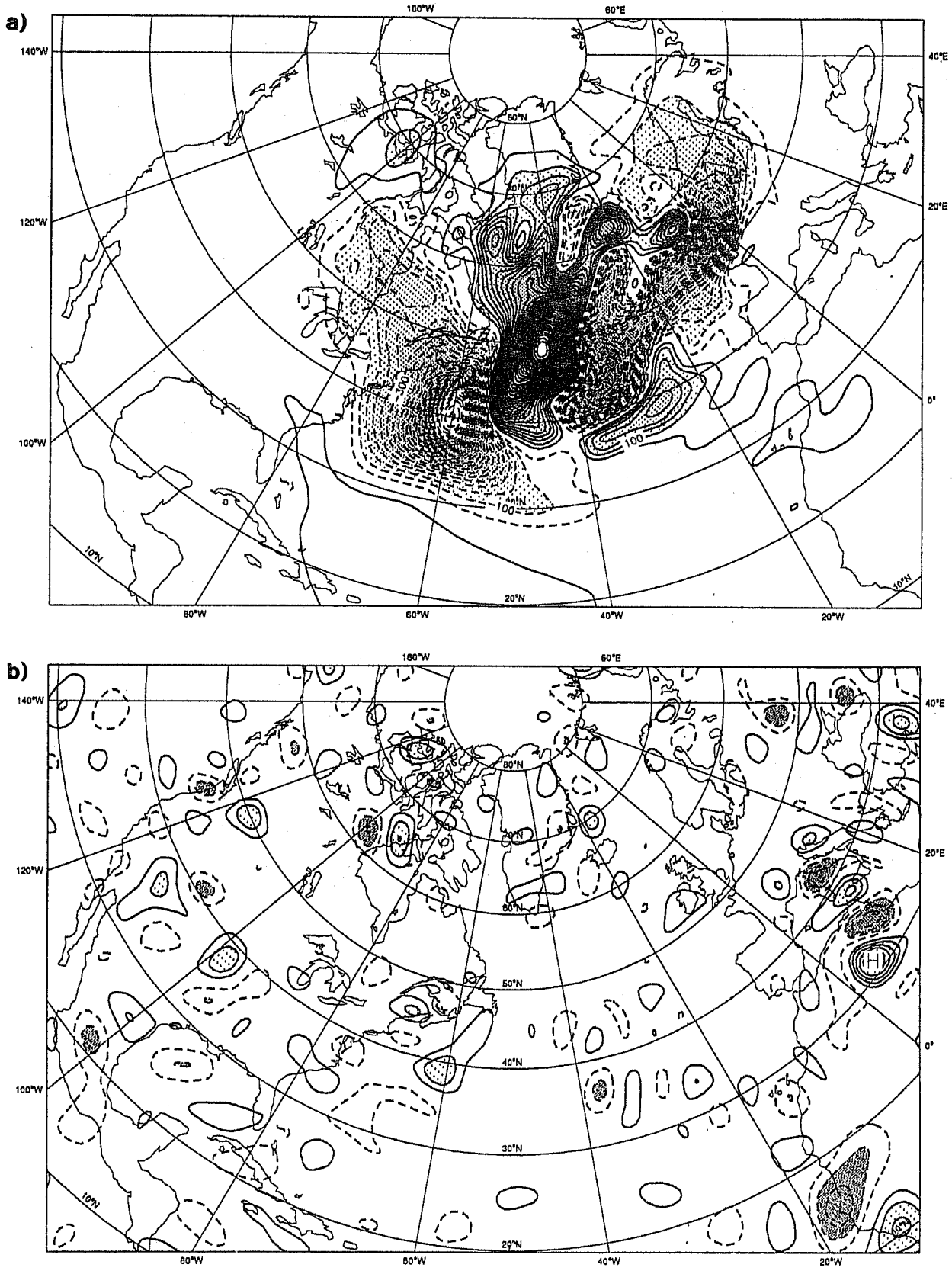

Fig 18 Panel a): gradient of 2-day forecast error diagnostic function with respect to the analysis valid for 3/4/93 (vorticity at level 26). Panel b): initialised analysis increments for 3/4/93 (vorticity at level 26). Panels c) and d): Analysed MSL pressure with corresponding observations for 3/4/93, 12Z and 4/4/93, 0Z. Panel e): initial perturbation added to the control of the Monte-Carlo system at 3/4/93 for the geopotential at 500 hPa which leads to the best score over the North-Sea for the 9/4/93.

c)

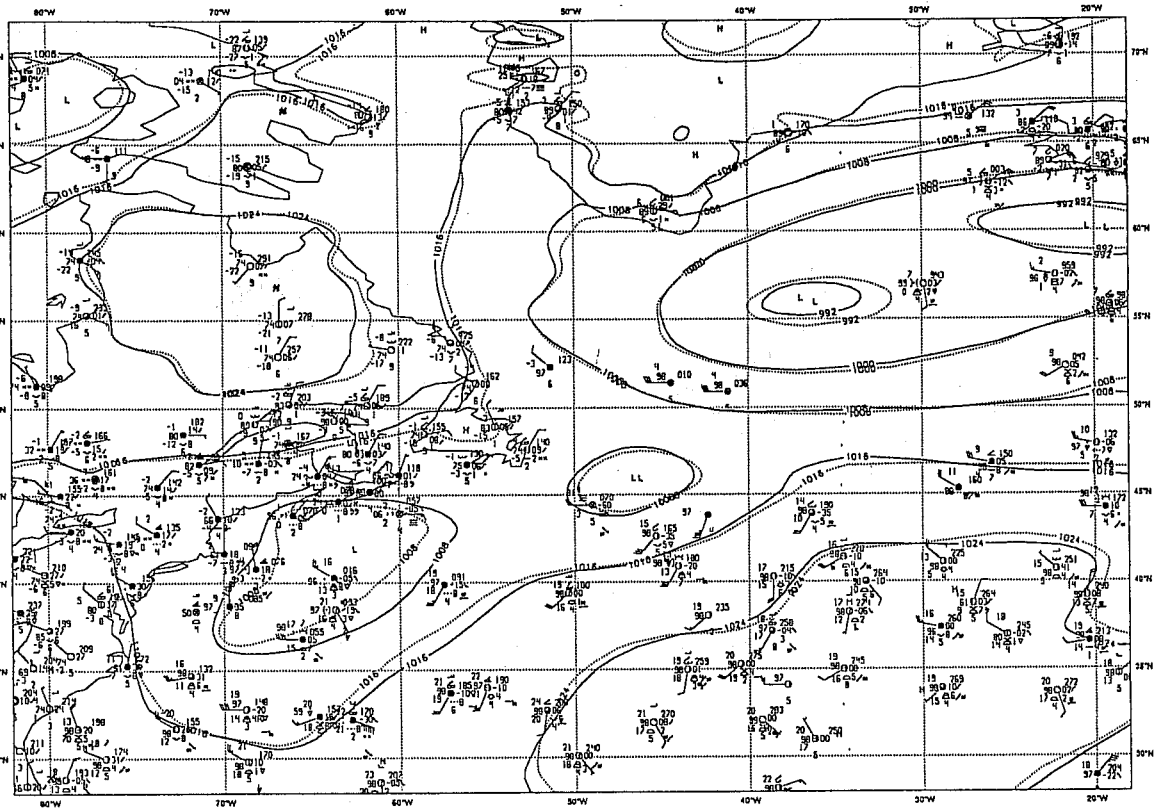

d)

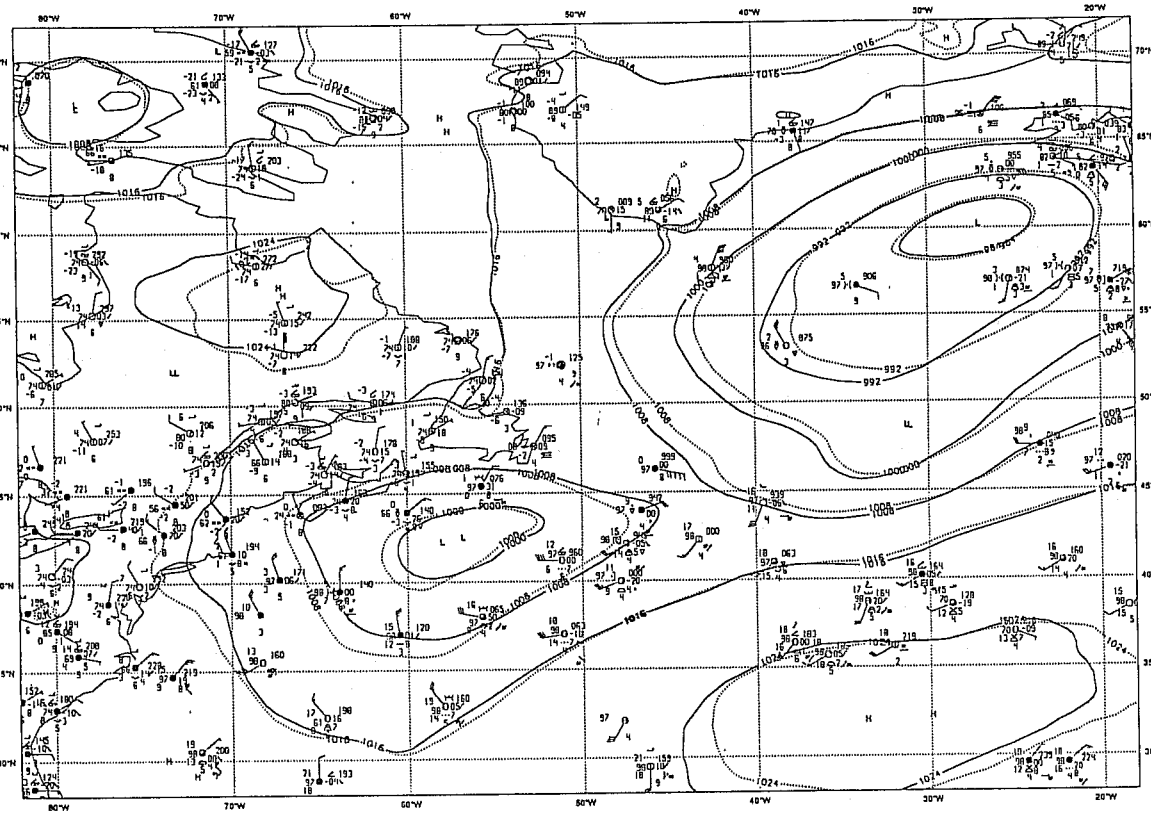

Fig. 18 continued

f) SPREAD - NDAY= 0- DF= 0.10000E+02

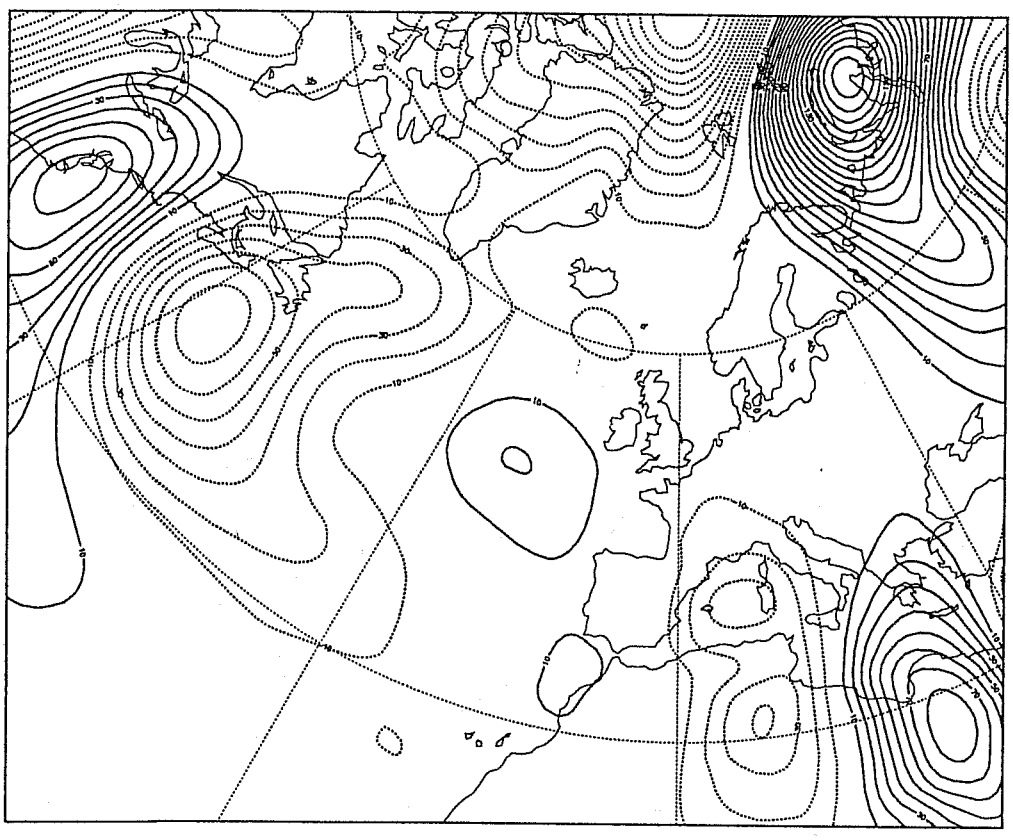

Fig. 18 continued

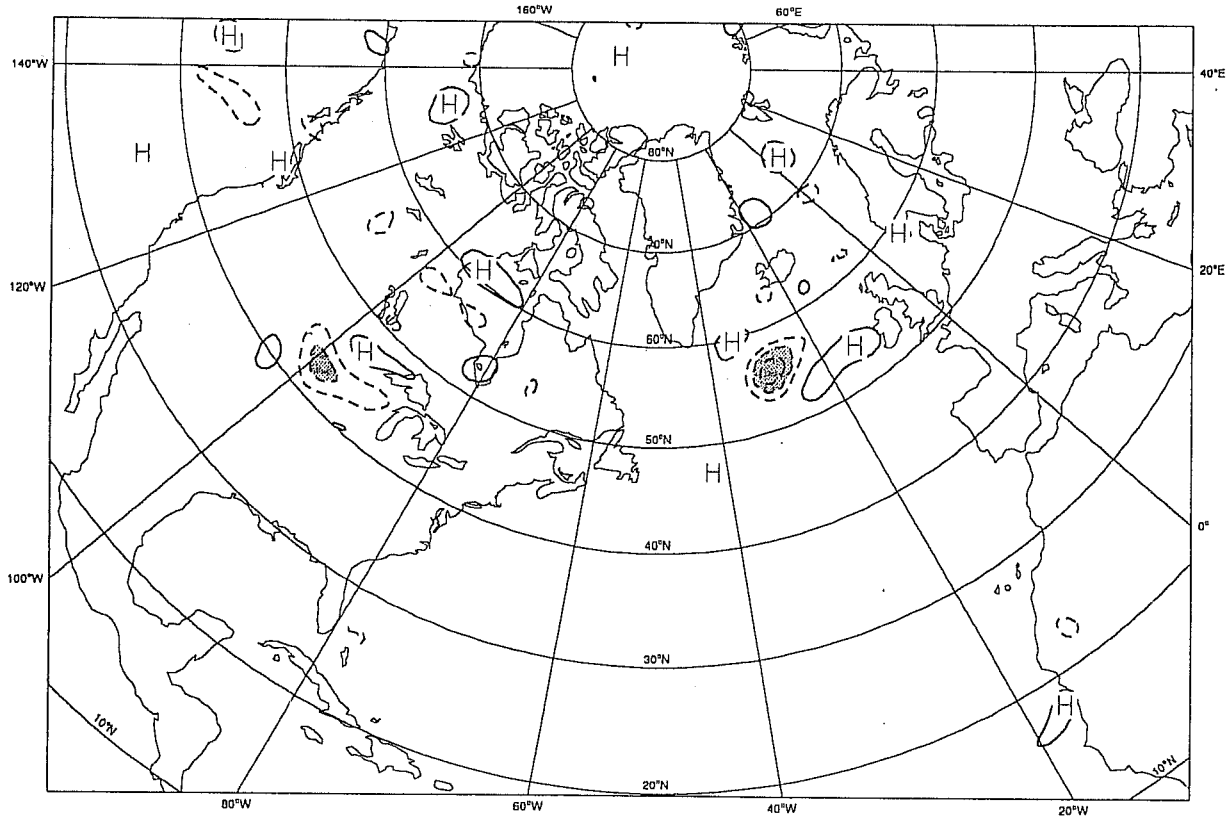

Fig 19 2-day forecast error for 14/9/92, 12Z, for vorticity at level 26 (850 hPa).

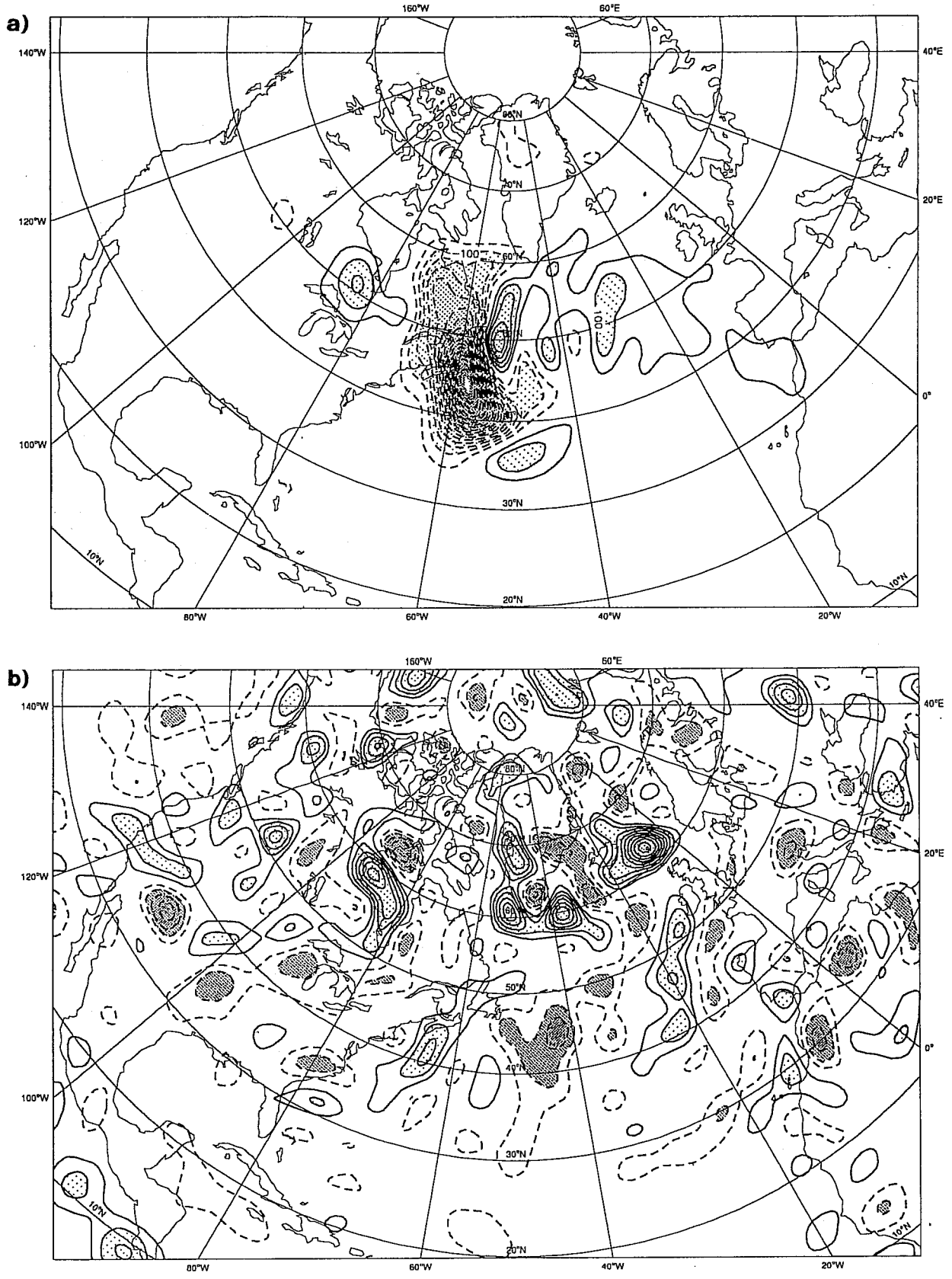

Fig 20 Panel a): gradient of 2-day forecast error diagnostic function with respect to the analysis valid for 12/9/92 (vorticity at level 26). Panel b): analysis valid for 12/9/92, 12Z (vorticity at level 26).